International Journal of Computational andExperimentalScience and ENgineering (IJCESEN)

Vol. 10-No.3 (2024) pp. 335-340
http://www.ijcesen.com

ISSN:2149-9144

Research Article

The distribution of shoulder enhancement and associated features among NEIALs spectra observed with the EISCAT Svalbard 42m radar

Bashkim DALIPI[1], Naim SYLA[2*], Fisnik ALIAJ[3], Donat DALIPI[4] and Arbër ZEQIRAJ[5]

[1]Public University Kadri Zeka, Faculty of Education, rr."ZijaShemsiu" pn. 60000 Gjilan, Republic of Kosovo
Email:bashkim.dalipi@uni-gjilan.net - **ORCID:**0000-0002-8133-0452

[2]University of Prishtina, Department of Physics, Eqrem Çabej Str. 51, 10000 Prishtina, Republic of Kosovo
* **Corresponding Author Email**: naim.syla@uni-pr.edu - **ORCID:**0000-0003-0857-4685

[3]University of Prishtina, Department of Physics, Eqrem Çabej Str. 51, 10000 Prishtina, Republic of Kosovo
Email: fisnik.aliaj@uni-pr.edu-**ORCID**:0000-0002-9967-8334

[4]Public University Kadri Zeka, Faculty of Education, rr."ZijaShemsiu" pn. 60000 Gjilan, Republic of Kosovo
Email:donat.dalipi.st@uni-gjilan.net - **ORCID:**0009-0002-8709-3037

[5]University of Mitrovica, Department of Materials and Metallurgy, PIM-Trepça, Mitrovica - Republic of Kosovo
Email:arber.zeqiraj@umib.net- **ORCID:**0000-0002-8615-6641

Article Info:

DOI:10.22399/ijcesen.347
Received : 18 June 2024
Accepted : 01 August 2024

Keywords:

Ionosphere
Ionospheric physics
Incoherent scatter radar
Power spectral density

Abstract:

Reports link Naturally Enhanced Ion Acoustic Lines (NEIALs) phenomena to ionospheric plasma processes, yet their full understanding remains unexplored. One of the reasons is that the plasma analysis using the Grand Unified Incoherent Scatter Data Analysis Program (GUISDAP) fails on occasions when these phenomena occur. However, we can evidence some aspects of the spectra, such as appearance, morphology, frequency of occurrence, and spectrum features, by analyzing the raw data using the Real-Time Graph (RTG) program. We obtained these data using the 42-meter EISCAT Svalbard radar. This article talks about the features of NEIALs, such as their spectral shape, enhanced spectral signatures, altitude distribution of spectral enhancement, frequency of NEIAL occurrence, maximum power returned, shoulder asymmetry enhancement, and frequency shift of the whole ion line spectrum. Additionally, we have discussed NEIALs characteristics related to specific ionospheric E and F regions.

1. Introduction

The theory of plasma incoherent scattering leads to a final equation that shows the power spectrum density of the radiation that is scattered by free electrons in the ionosphere. These spectra record the properties of the ionospheric plasma. The incoherent scatter radar technique dumps the ionospheric backscattered signal as raw data. The total power spectral density has two parts: the ion part and the electron part. The ion part of the spectral density has a unique shape and size, with two double-humped shoulders that are down-shifted and up-shifted and partly superimposed. They are situated just around the radar beam's frequency [1]. The plasma part, on the other hand, is on both sides of the frequency of the radar beam, but a few MHz away from it, to the left and right of the frequency of the radar beam. According to Lunde et al. [2], the ion lines correspond to ion-acoustic waves propagating toward and away from the receiving radar antenna.
The ion part of the spectra reacts very sensitively according to the changes in physical parameters in the ionosphere. Figure 1 shows an example of the ion line shapes and sizes that correspond to the power scattered by oxygen (O+), assuming Maxwellian plasma. Previous studies have reported different features of incoherent radar spectra in the domain of statistics [3, 4, 5, 6]. Furthermore, studies have linked NEIALs to an increase in plasma electron temperature [3, 7]. In this paper, we will organize, summarize, and interpret the information regarding the morphological variations of power spectral density contained in raw data collected with the European Incoherent Scatter Radars (EISCAT).

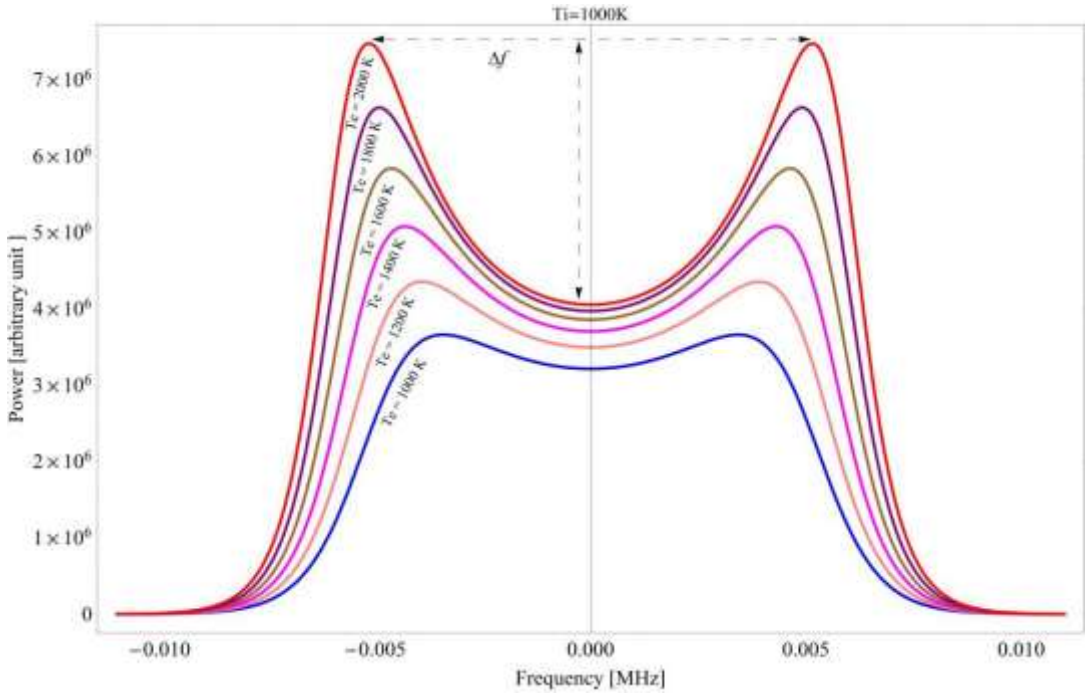

***Figure 1**. Ion line shapes for oxygen (O+) taking into account ion temperature (Ti = 1000 K) while applying different electron temperatures (Te = 1000 K, Te = 1200 K, Te = 1400 K, Te = 1600 K, Te = 1800 K, and Te = 2000 K).*

In this paper, we will organize, summarize, and interpret the information regarding the morphological variations of power spectral density contained in raw data collected with the European Incoherent Scatter Radars (EISCAT).

2. Material and methods

EISCAT Svalbard Radar (ESR): On June 1, 2024, the EISCAT Svalbard Incoherent Scatter Radar at Longyearbyen, located at approximately 78 degrees North and 16 degrees East (geographically), produced the target data used in our observation. The radar antenna was 42 m in diameter, fixed, field-aligned, and had an emitting and receiving capability. The working frequency for this radar was 500 MHz.

Rutherford Appleton Laboratory (RAL): The computer network at RAL (England) serves as an archive, continuously depositing the EISCAT raw data. Accessing the data is restricted. We asked the authorities at RAL to allow access to RAL databases in order to exploit the raw data sets for scientific and non-commercial purposes.

Real-Time Graph (RTG): This Matlab program plots incoming data in real time. RTG runs in post-experiment mode, too (http://www.eiscat.se/rtg/remtg.html). The ESR 42m Real Time Graph (RTG) program is capable of generating, as an output, a spectral panel and a power panel that change in terms of shape and size in response to backscattered incoherent radar signals. Our experiment used a MATLAB-based definition file called rtg_tau0_510.m.

3. Results and discussion

Our goal was to figure out how the power spectral density changed shape and size over time. We examined a series of 5141 6.4-second data dumps created on June 1, 2024, from 7:22:55 UT to 18:01:07 UT, to achieve this. These data dumps represent a total of 9.14 hours of space scans performed by the ESR 42 m radar. During our observation, there were some time slices when the radar was in a turned-off state. That time represented, in total, about 1.5 hours. The radar's transmitter-off state produced noisy data dumps that lacked information on ionospheric plasma properties.

We distinguished between the three major morphological features of the spectra (i.e., shapes and sizes) through visual inspections of raw data dumps, analytical analysis, and comparative analysis. Those are: (1) the normal morphology, (2) NEIALs morphology, and (3) the hard-object morphology [8]. Figure 2 shows one example of the spectra, characterized by three very distinct morphologies.

NORMAL morphology evidence:

The normal morphology appears in the spectral panel of PSD as a result of the scattering properties of the ionosphere, where the distribution of speeds of plasma particles is Maxwellian or is close to

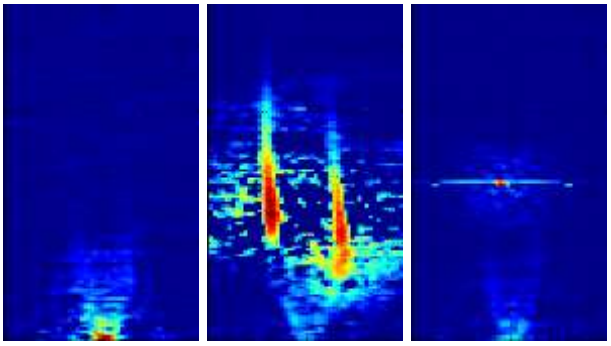

A normal morphological sample | NEIALs morphology sample | Hard-object morphology sample

***Figure 2**. The power spectral density (PSD) and the three main spectral morphological classes. The x-axis represents the frequency offset (kHz), while the y-axis represents the altitude range (km).*

Maxwellian. We counted a total of 4170 data dumps (81.11 percent) that showed normal morphologies. Figure 3 (left panel) shows the dominance of the normal morphology among observed data dumps. This is an indication that most of the time, the probed ionospheric plasma medium showed a Maxwellian distribution of speeds.

HARD-OBJECT morphology evidence:
Enhanced returns that came from a very limited altitude range were assumed to be scattering from a hard target, such as a satellite [9]. We suspect that satellites or space debris passing through the main beam or side lobes are responsible for many of the hard object cases found in the spectra [10]. We found that power returns from hard objects impacted a total of 941 data dumps, accounting for 18.3 percent. Furthermore, we have counted and grouped the consecutive data-damp sequences whose spectral morphologies are affected by the same hard object (artificial satellites, space debris, etc.).
NEIALs morphology evidence: Large enhanced returns that were extended in altitude along the geomagnetic field were assumed to be of geophysical origin [9]. We classified only 30 data dumps (0.58 percent) as power returns caused by geophysical processes. We classified the development and signature of a NEIALs process in one or a few consecutive data dumps as either an event or a correlated event [8]. Out of the 30 NEIALs that were seen, only two happened in a single data dump. In the other two cases, the NEIALs event happened in two consecutive data dumps.

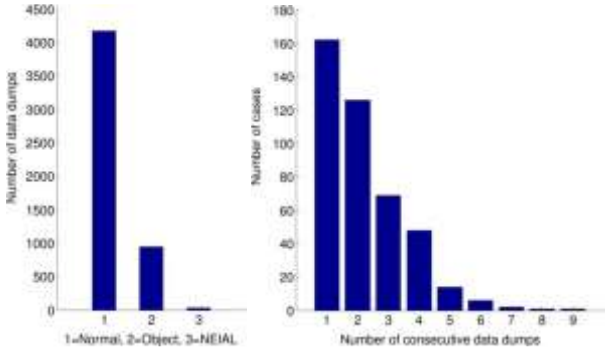

***Figure 3**. Left graph: Among the 5141 data dumps observed, normal morphology was dominant. Hard objects (satellites, space debris, etc.) were very common, and a number of NEIALs were observed.*
Right graph: Among the 941 data damps signed by hard object power returns, the frequency dominated a single data dump (162 cases), followed by two consecutive data damps (126 cases), then three consecutive data damps (69 cases), and so on.

In one case, it happened in three consecutive data dumps. In four cases, it happened in four consecutive data dumps, and in one case, it happened in five consecutive data dumps. In our observations, we have seen enhancements that dominated the left, the right, or both shoulders simultaneously.
Table 1 displays the primary attributes of each data dump classified as NEIALs, while Figure 4 shows the comparison between the altitude of maximum enhancement for the down-shifted shoulder and the up-shifted shoulder.

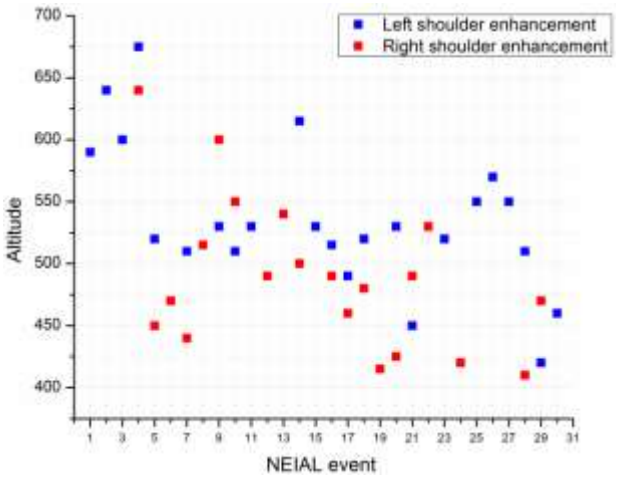

***Figure 4**. Distribution of maximum shoulder enhancement by altitude for each NEIALs sequence observed (30 total). At lower altitudes, the maximum right shoulder enhancement dominates, while at higher altitudes, the maximum left shoulder enhancement dominates.*

Table 1.*The primary attributes of each data dump classified as NEIALs.The altitude range, both down-shifted and up-shifted, determines the maximum power return at that particular altitude. The asterisk symbol denotes the altitude range for maximum enhancement, indicating which shoulder is more enhanced.*

NEIAL Event number observed (event intensity)	**Data dump integration (UT)**	**Altitude of maximum enhancement for the down-shifted shoulder (km)**	**Altitude of maximum enhancement for the up-shifted shoulder (km)**	**Maximum of the power returned (K)**	**Shoulder enhancement dominance for particular data dump integration**	**Spectral shift in the domain of frequency**
1 (weak)	07:31:08 UT	590*	no enhance	0< P < 100	down-shift	left
	07:31.15 UT	640*	no enhance	0< P < 100	down-shift	left
	07:31:21 UT	600*	no enhance	0< P < 100	down-shift	left
	07:31:27 UT	675	640*	0< P < 100	up-shift	left
2 (strong)	07:35:56 UT	520	450*	380	up-shift	left
	07:36:03 UT	470*	470	6000	down-shift	left
	07:36:09 UT	510*	440	19000	down-shift	left
	07:36:16 UT	515*	515	1500	down-shift	left
3 (moderate)	07:36:41 UT	530	600*	130	up-shift	left
	07:36:48 UT	510*	550	650	down-shift	left
4 (weak)	07:43:05 UT	530*	no enhance	0< P < 100	down-shift	center
5 (weak)	08:03:15 UT	no enhance	490*	0< P < 100	up-shift	center
6 (moderate)	08:03:47 UT	no enhance	540*	0< P < 100	up-shift	center
	08:03:53 UT	615	500*	180	up-shift	center
7 (strong)	08:07:44 UT	530*	no enhance	150	down-shift	left
	08:07:50 UT	515	490*	150	up-shift	left
	08:07:56 UT	490	460*	1200	up-shift	left
	08:08:03 UT	520*	480	5300	down-shift	left
8 (strong)	08:16:09 UT	no enhance	415*	200	up-shift	center
	08:16:15 UT	530	425*	200	up-shift	center
	08:16:22 UT	450*	490	1400	down-shift	center
	08:16:28 UT	no enhance	530*	0< P < 100	up-shift	center
9 (moderate)	08:19:27 UT	520*	no enhance	0< P < 100	down-shift	left
	08:19:34 UT	no enhance	420*	200	up-shift	center
	08:19:40 UT	550 *	no enhance	0< P < 100	down-shift	left
	08:19:47 UT	570*	no enhance	0< P < 100	down-shift	left
	08:19:53 UT	550*	no enhance	0< P < 100	down-shift	left
10 (strong)	11:59:12 UT	510	470*	1900	up-shift	center
	11:59:18 UT	420*	410	670	down-shift	center
	11:59:24 UT	460*	no enhance	0< P < 100	down-shift	center
		533 km (average altitude)	**484 km** (average altitude)		**17** down-shifted versus **13** up-shifted	

We classified three of the 10 NEIALs events found in our data as weak plasma processes, three as moderate processes, and four as strong processes [8].

The power registered varied among the data dumps. The maximum power returned was approximately 19000 K, which corresponded to the second event (07:36:09 UT). In 17 of the 30 data dumps containing NEIALs, the down-shifted shoulder dominated, while in 13 of them, the up-shifted shoulder dominated. We set the average altitude height to 533 km for the down-shifted shoulder and 484 km for the up-shifted shoulder, corresponding to the maximum enhancement.
We found that the altitude range and the spectral asymmetry can change completely between successive data dumps. For instance, we observe this between 08:07:56 UT and 08:08:03 UT, or between 11:59:12 UT and 11:59:18 UT. This is in good agreement with the previous reports [4].

Our observations showed that the down-shifted NEIALs realize their maximum intensity in the F region of the ionosphere. This is in good agreement with findings by Ogawa et al. [6], who concluded that the down-shifted NEIALs are usually stronger above an altitude of 300 km.

From Table 1, we can conclude that the up-shifted NEIALs realize their maximum intensity around 50 km below the down-shifted NEIALs, but this region still lies within the F region of the ionosphere. This part of our findings is not in agreement with findings by Ogawa et al. [6], who stated that the up-shifted NEIALs dominate in the E region. In the thirty NEIAL profiles we found, none of the up-shifted NEIALs had the maximum intensity in the E region of the ionosphere, even though some extended from the F region to the E region. The number of NEIAL profiles we used for the statistics (30 total) could potentially influence this disagreement. In terms of the whole spectral shift, we found that the ion line enhancements, down-shifted in frequency, dominated the statistics (see Table 1, last column).

4. Conclusions

Three main types of morphologies have been considered: (1) the normal morphology, (2) the NEIALs morphology, and (3) the hard-object morphology. Our observations showed that the normal spectra were the most common (81.11%), followed by hard object-affected spectra (18.3%), and then a small number of NEIALs spectra (0.58%).
A particular NEIALs event, as well as a hard object event, could develop within one data dump in time scales not exceeding 6.4 s. We also discovered that both NEIALs and hard-object events could develop over multiple consecutive data dumps, with time scales exceeding 6.4 s. Our observations showed that the down-shifted NEIALs, as well as the up-shifted NEIALs, realized their maximum intensity in the F region. On average, the up-shifted NEIALs realized their maximum intensity around 50 km below the down-shifted NEIALs. In the thirty NEIAL profiles we found, none of the up-shifted NEIALs had the maximum intensity in the E region of the ionosphere, even though some extended from the F region to the E region. In terms of the whole spectral shift, we found that the ion line enhancements, down-shifted in frequency, dominated the statistics.

Author Statements:

- **Ethical approval**: The conducted research is not related to either human or animal use.
- **Conflict of interest:** The authors declare that they have no known competing financial interests or personal relationships that could have appeared to influence the work reported in this paper.
- **Acknowledgement:** EISCAT is an international association supported by research organizations in China (CRIRP), Finland (SA), France (CNRS, till end 2006), Germany (DFG), Japan (NIPR and STEL), Norway (NFR), Sweden (VR), and the United Kingdom (STFC). The data used in this paper is the property of EISCAT. We are particularly grateful to the UK EISCAT Support Group at Rutherford Appleton Laboratory for allowing access to the data.
- **Author contributions:** The authors declare that they have equal rights to this paper.
- **Funding information:** The authors declare that there is no funding to be acknowledged.
- **Data availability statement:** The data that support the findings of this study are available on request from the corresponding author. The data is not publicly available due to privacy or ethical restrictions.

References

[1] Gordon, W. (1958). Incoherent Scattering of Radio Waves by Free Electrons with Applications to Space Exploration by Radar. *Proceedings of the IRE*, *46*(11), 1824–1829. https://doi.org/10.1109/jrproc.1958.286852

[2] Lunde, J., Løvhaug, U. P., & Gustavsson, B. (2009). Particle precipitation during NEIAL events: simultaneous ground based nighttime observations at

Svalbard. *Annales Geophysicae*, *27*(5), 2001–2010. https://doi.org/10.5194/angeo-27-2001-2009

[3] Rietveld, M. T., Collis, P. N., & St- Maurice, J. (1991). Naturally enhanced ion acoustic waves in the auroral ionosphere observed with the EISCAT 933-MHz radar. *Journal of Geophysical Research*, *96*(A11), 19291–19305. https://doi.org/10.1029/91ja01188

[4]Rietveld, M., Collis, P., vanEyken, A., &Løvhaug, U. (1996). Coherent echoes during EISCAT UHF Common Programmes. *Journal of Atmospheric and Terrestrial Physics*, *58*(1–4), 161–174. https://doi.org/10.1016/0021-9169(95)00027-5

[5] Ogawa, Y., Buchert, S. C., Fujii, R., Nozawa, S., &Forme, F. (2006). Naturally enhanced ion-acoustic lines at high altitudes. *Annales Geophysicae*, 24(12), 3351–3364. https://doi.org/10.5194/angeo-24-3351-2006

[6]Ogawa, Y., Buchert, S. C., Häggström, I., Rietveld, M. T., Fujii, R., Nozawa, S., & Miyaoka, H. (2011). On the statistical relation between ion upflow and naturally enhanced ion-acoustic lines observed with the EISCAT Svalbard radar. *Journal of Geophysical Research*, *116*(A3). https://doi.org/10.1029/2010ja015827

[7] Dalipi, B., Syla, N., & Aliaj, F. (2020). Electron Temperature Fluctuations on the Eve and after the NEIAL Events Observed with the EISCAT Svalbard Radar. *Acta Physica Polonica. A*, *137*(4), 509–512. https://doi.org/10.12693/aphyspola.137.509

[8] Dalipi, B. (2013). The Morphology of Naturally Enhanced Ion-acoustic Lines Observed in ESR 42m Data. *Journal of Scientific Research and Reports*, *3*(1), 234–254. https://doi.org/10.9734/JSRR/2014/5695

[9] Michell, R. G., Lynch, K. A., Heinselman, C. J., &Stenbaek-Nielsen, H. C. (2008). PFISR nightside observations of naturally enhanced ion acoustic lines, and their relation to boundary auroral features. *Annales Geophysicae*, *26*(11), 3623–3639. https://doi.org/10.5194/angeo-26-3623-2008

[10] Porteous, J., Samson, A. M., Berrington, K. A., & McCrea, I. W. (2003). Automated detection of satellite contamination in incoherent scatter radar spectra. *Annales Geophysicae*, *21*(5), 1177–1182. https://doi.org/10.5194/angeo-21-1177-2003